Path-integral Monte Carlo simulation of helium at negative pressures

Gregory H. Bauer, David M. Ceperley, and Nigel Goldenfeld
Department of Physics, University of Illinois, 1110 West Green Street, Urbana, Illinois 61801-3080
(Received 20 August 1999; revised manuscript received 17 November 1999)

Path-integral Monte Carlo simulations of liquid helium at negative pressure have been carried out for a temperature range from the critical temperature to below the superfluid transition. We have calculated the temperature dependence of the spinodal line as well as the pressure dependence of the isothermal sound velocity in the region of the spinodal. We discuss the slope of the superfluid transition line and the shape of the dispersion curve at negative pressures.

I. INTRODUCTION

Consider a liquid that is quenched from above the liquid-gas coexistence line to a point below, which will be in either the metastable or unstable region, see Fig. 1. As it approaches equilibrium, the system will phase separate to a state of positive pressure with coexisting vapor and liquid phases of densities ρ_v and ρ_l, respectively. Below this coexistence line is the spinodal line, which delineates the metastable phase from the unstable phase. The spinodal line is the locus of points where the speed of sound vanishes $m_4 c^2 = \partial P/\partial \rho$, where m_4 is the mass of a ^{4}He particle. At the spinodal there is no energy barrier to nucleation and phase separation. If the temperature is low enough the pressure at the liquid spinodal, at a density of ρ_{sl}, may be negative. Once the spinodal pressure becomes negative, the lowest pressure the system can attain is the spinodal pressure.

Direct measurement of the spinodal pressure of liquid helium by homogeneous nucleation is experimentally difficult. In a driven system, such as the pressure oscillation experiments of Maris[1,2] and Balibar,[3,4] negative pressures are only achieved for a finite duration. The presence of objects such as vortices,[5] electrons,[6,7] or both[8] lower the nucleation energy barrier. Measurements of the cavitation pressure are higher than the spinodal pressure because of quantum tunneling[9] or thermal activation[10] over the barrier, but are consistent with predictions of the nucleation energy barrier, attempt frequency and the spinodal pressure. In this paper microscopic path-integral Monte Carlo (PIMC) simulations of liquid helium at negative pressure and finite temperature will be presented. The calculated temperature and density dependence of the spinodal line compare favorably with other calculations.[11–17] We show that the superfluid transition can be extended to negative pressures. Finally, the density dependence of the excitation spectrum shows a decrease in the maxon peak and an increase of the roton minimum as the liquid spinodal is approached.

II. METHOD

At zero temperature, density-functional[11,16] and microscopic-phenomenological[15,17] calculations and quantum Monte Carlo (QMC) (Refs. 13,14) simulations of liquid helium at negative pressure have produced comparable values of the spinodal pressure and density. At finite temperature, a density functional[11] developed for the liquid-gas interface has been used to successfully examine helium at negative pressures. Microscopic finite temperature simulations at negative pressures have not been performed until now.

It has been well documented that PIMC can provide accurate thermodynamic and some dynamical properties of quantum systems in equilibrium, and has been especially successful with liquid helium.[18,19] The basis for the path integral method is the evaluation of the many particle density matrix $\rho = \exp(-\beta \mathcal{H})$. The Hamiltonian is assumed to be

$$\mathcal{H} = -\lambda \sum_{i=1}^{N} \nabla_i^2 + \sum_{i<j} v(r_{ij}), \tag{1}$$

where an accurate two-body interaction $v(r)$ (Ref. 20) is used. From the density matrix, expectation values of observables can be determined

$$\langle O \rangle = Z^{-1} \int dR dR' \rho(R,R') \langle R' | O | R \rangle, \tag{2}$$

with the partition function Z

$$Z = \int dR \rho(R,R), \tag{3}$$

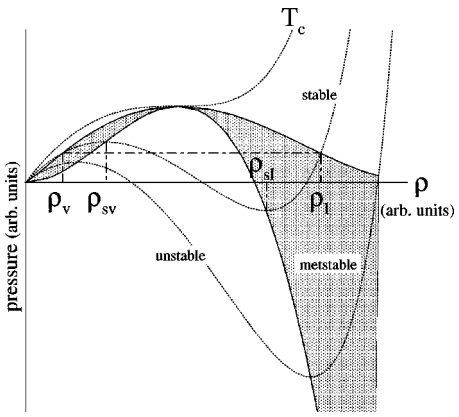

FIG. 1. Isotherms of pressure versus density for a generic liquid are shown for temperatures at or less than the critical temperature. The spinodal line and the coexistence line form the lower and upper bounds of the shaded metastable region. Locations of the saturated vapor and liquid densities ρ_v and ρ_l, and the spinodal vapor and liquid densities ρ_{sv} and ρ_{sl}, for a given isotherm are indicated.

and where the matrix elements of the density matrix in position basis is

$$\rho(R,R')=\langle R|e^{-\beta\mathcal{H}}|R'\rangle. \quad (4)$$

R is the $3N$ state of the system, $R=\{r_1,r_2,..r_N\}$. Using the product property, the density matrix can be expressed as

$$e^{-\beta\mathcal{H}}=(e^{-\tau\mathcal{H}})^M, \quad (5)$$

where $M_\tau=\beta=1/k_BT$ and τ is the imaginary time step. By expressing the density matrix at T as a product of density matrices at a higher temperature of MT, Eqs. (2) and (4) can be accurately evaluated by Monte Carlo. In our simulation, the canonical ensemble is used, with a fixed number of particles N, simulation volume and temperature T. For ^{4}He, $\lambda=6.05961\,\mathrm{K\,\AA^2}$, and during the simulations $\tau=0.0125\,\mathrm{K}^{-1}$ and $N=64$. PIMC incorporates Bose statistics, necessary for the modeling of superfluid ^{4}He, by allowing the permutation of particle paths. Superfluidity manifests itself as the winding[21] of the particle paths across the simulation cell when periodic boundaries are present.

An advantage of a finite system is its ability to explore systems at negative pressures. A disadvantage is that finite-size effects are present, which can be appreciable for a small system and can be difficult to correct. The liquid-gas interface limits how large a system can be simulated due to the surface energy of a phase separated system. Because the simulation is in equilibrium it will phase separate if it is thermodynamically favorable. Choosing a system size that is on the order of the liquid-gas interface width prevents the system from forming a stable coexistence. From previous PIMC simulations[18] it was found that a 64 particle system is large enough to provide accurate bulk properties. To check that this holds true near the spinodal, the pressure near the spinodal was examined for several systems from 8 to 256 particles at a temperature of 2.0 K. In the range of 32 to 128, the pressure remained negative and varied little with particle number, and $S(k)<1$ for small k (see below). A system of 64 particles was found to be optimal for minimizing finite-size effects and keeping the fluid homogeneous at negative pressure.[17]

To differentiate between liquid and gas phases, the static structure function $S(k)$ and the pair distribution function $g(r)$ were examined at three representative densities. Information about fluctuations into the coexisting liquid-gas phase, which we wish to avoid, is present in both $S(k)$ and $g(r)$. In Fig. 2 the two functions are shown for three densities and a temperature of 2.0 K. The high-density liquid phase and the low-density gas phase show the typical features in $S(k)$ and $g(r)$. The intermediate density, which is lower than the liquid spinodal density at that temperature, begins to show signs of phase separation but no large scale features [$S(k)\gg 1$ for small k] are present. As the density is varied from liquid to gas the functions should go smoothly from one phase to the other, for a finite system.

III. ANALYSIS

A. Spinodal line

The PIMC density-pressure isotherms are plotted in Fig. 3. To determine the location of the liquid spinodal line, a cubic polynomial in density was fit to each density-pressure isotherm in the region of the liquid spinodal. As will be shown below, the cube of the isothermal speed of sound is seen to vary linearly with pressure and from this it can be shown that $P\sim P_{sl}+\alpha(\rho-\rho_{sl})^3$ near the liquid spinodal.[12] In Table I the liquid spinodal pressure and density for various temperatures are listed and are plotted in Fig. 3. These points are indicated by the filled circles. The χ^2 goodness of fit is on the order of 1 for low temperatures and on the order of 2 at the highest temperatures. Simulations of the gas phase were not done for all temperatures and so information about the gas spinodal and the liquid-gas coexistence densities is not available.

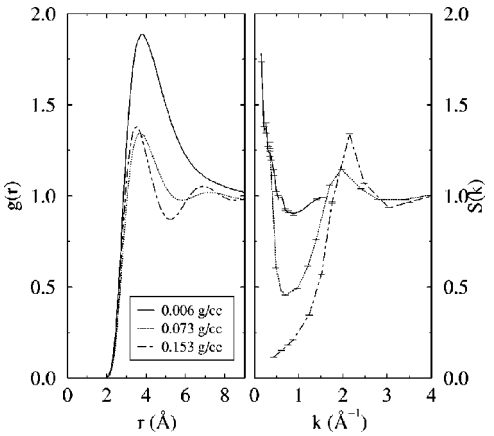

FIG. 2. The pair correlation function and the static structure function are shown for three densities at a temperature of 2.0 K: 0006 g/cc, 0.073 g/cc, and 0.153 g/cc.

For comparison, density-functional,[11,16] extrapolated experimental,[12] optimized hypernetted chain,[17] and QMC (Ref. 14) values are shown in Fig. 3. The extrapolated values depend on the assumption that the isothermal speed of sound has the following power-law dependence, $c^3\sim P-P_{sl}$, where P_{sl} is the liquid spinodal pressure. The density-functional values are the result of a parametrized density functional that reproduces the experimental bulk properties but with the Bose condensation added *post hoc*. While there

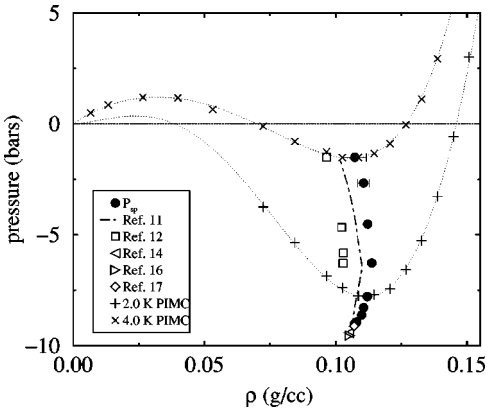

FIG. 3. Spinodal pressure from PIMC simulations are compared to other calculations and estimations of the spinodal pressure. Increasing temperature runs from bottom to top. Two isotherms from PIMC simulations are shown as well, with dotted lines to guide the eye.

TABLE I. ^{4}He liquid spinodal values.

T (K)	ρ_{sl} (g/cc)	P_{sl} (bars)
0.50	0.1070(51)	−8.99(3)
1.00	0.1077(45)	−8.93(3)
1.54	0.1097(38)	−8.62(3)
1.74	0.1110(51)	−8.28(4)
2.00	0.1123(45)	−7.77(3)
2.50	0.1136(51)	−6.27(3)
3.00	0.1123(51)	−4.52(1)
3.64	0.110(14)	−2.68(6)
4.00	0.107(28)	−1.51(1)

is agreement with the temperature dependence of the liquid spinodal pressure, the PIMC values of the liquid spinodal density tend to be higher than the density-functional and extrapolated values. Linearly extrapolating the PIMC data to 0 K yields a spinodal density very close to the QMC, density functional and hypernetted chain values. The extrapolated 0 K PIMC spinodal pressure is slightly larger than the other 0 K results. A possible reason for this discrepancy, at least with the QMC value, is the use of different versions of the Aziz pair potential.[29]

In Fig. 4 the temperature dependence of the liquid spinodal pressure, as calculated by PIMC, is plotted. For T in the neighborhood of the critical temperature T_c, the spinodal pressure behaves similar to that of a Van der Waals gas with the spinodal pressure decreasing monotonically with decreasing temperature. In this region we see good agreement of the spinodal pressures. At temperatures near zero, the spinodal pressure is approximately independent of temperature, being slightly higher than other values when extrapolated to 0 K. This flat region may be understood in terms of the quasiparticle picture of liquid helium[12] and will be discussed below. At temperatures near 2 K there is a distinct transition between the two regions. In comparison, the density functional values of Ref. 11 of the spinodal pressure vary smoothly from the zero temperature value to the classical gas behavior, having no flat region at low temperatures.

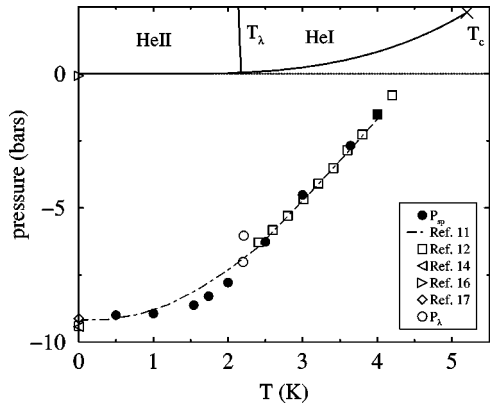

FIG. 4. Temperature dependence of the spinodal pressures and the superfluid transition at negative pressures are shown. At low temperatures the spinodal pressure is insensitive to temperature while at higher temperatures the behavior is linear. The upper solid lines form usual phase diagram.

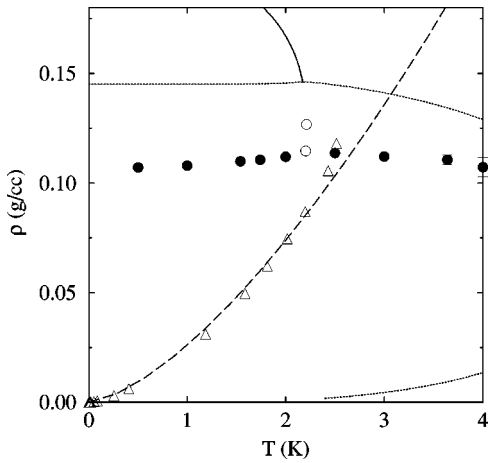

FIG. 5. The temperature dependence of the spinodal density (●) and transition density (○) are shown with the experimental coexistence curve (dashed line) and superfluid transition curve (solid line). The spinodal density exhibits a cusp-like feature as it intersects the superfluid transition curve. The transition temperature for the hard sphere Bose gas of Ref. 25 (△) and the ideal Bose gas (long dashed line) are shown for comparison.

The extrapolated experimental spinodal pressures of Hall and Maris[12] were limited to temperatures above 2.2 or at 0 K.

It is illustrative to plot the liquid spinodal density versus temperature, as is shown in Fig. 5. The liquid spinodal density shows a temperature dependence similar to the experimental liquid coexistence density (dashed line): a temperature independent region at low temperatures with a slight cusp *like* behavior near where the experimental transition line (solid line) approaches. The transition line at negative pressures as determined from PIMC simulation is discussed below.

B. Superfluid transition

It is not clear what is the temperature dependence of the superfluid transition line at negative pressures.[17,12] Experimentally, at positive pressures, as the density is reduced, the transition temperature increases. Further reducing the density, the transition line could extend into the negative pressure region. Additionally, along an isotherm, as the density is reduced to the spinodal density, superfluidity will vanish as the speed of sound vanishes.[17] In order to accurately determine the superfluid transition temperature we used finite-size scaling of the superfluid fraction.[22] The direct estimator for the superfluid fraction uses the winding number, which is a measure of the degree to which the particle exchange cycles form paths that span the width of the periodic cell.[23] For a finite N, the superfluid fraction should scale as

$$\frac{\rho_s(T)}{\rho} \sim L^{-1} Q(L^{1/\nu} t), \tag{6}$$

where $t=(T-T_\lambda)/T_\lambda$ is the reduced temperature. For the critical exponent of the correlation length ν experiment gives $\nu=0.67$. By assuming that the scaling function Q is linear with respect to its argument near $T=T_\lambda$, the parameters ν and T_λ can be varied to minimize the distance of the data to

TABLE II. Superfluid transition values.

T_λ (K)	ρ_λ (g/cc)	P_λ (bars)	ν	$\tilde{Q}(0)$[a]
2.20(2)	0.11463	−7.014(9)	0.63(4)	0.49(2)
2.21(2)	0.12669	−6.034(11)	0.65(4)	0.55(2)

[a] $\tilde{Q}(0)=\hbar^2\rho_\lambda^{2/3}Q(0)/m_4k_BT_\lambda$.

Q. The universal constant $\tilde{Q}(0)$, see Table II, has been calculated for the 3D XY model[24] as 0.49(1).

Using systems of 16, 32, and 64 particles at a fixed density, the superfluid fraction was determined at several temperatures and scaled according to Eq. (6). Once the transition temperature was found, the corresponding pressure was found by interpolating the $N=64$ pressure data. The superfluid transition values plotted in Figs. 4 and 5 are listed in Table II. The superfluid transition data fall along the experimental superfluid transition line if it extended linearly to negative pressures. It appears that the transition line intersects the spinodal line at a temperature of 2.2 K.

For comparison, the transition temperature for a hard sphere Bose gas[25] (a system which does not have a liquid-gas transition) and an ideal Bose gas are shown in Fig. 5. As was explained by Grüter[25] in a study of superfluidity for a hard sphere Bose gas, at low densities spatial fluctuations are important and clusters are likely to form, which inhibit macroscopic exchange cycles. At moderate densities the system is more homogeneous, allowing the exchange cycles necessary for superfluidity to form and the transition temperature becomes greater than the ideal Bose gas value by 7%. At high densities, exchange is once again inhibited due to an increase in effective mass of the particles lowering the transition temperature below the ideal Bose gas value. Note that in comparing the temperature dependence of the transition densities, the pressures of the ideal and hard sphere Bose gases are positive while the pressure of the ^{4}He transition goes from positive to negative as the density decreases.

C. Isothermal sound velocity

The scaling of experimental isothermal sound velocity data to pressure is controversial. Early thermodynamic arguments put forth by Maris[26] indicated that at $T=0$ K the speed of sound should scale with pressure as $c^4\sim P-P_{sl}$ where P_{sl} is the liquid spinodal pressure. Maris's later analysis[27,28] indicated that this was not correct in the pressure range accessible to experiment. A renormalization-group analysis of the problem by Maris[27] yielded a scaling relation of $c^3\sim P-P_{sl}$ for pressures near P_{sl}, which proved to be very representative of the data of both ^{4}He and ^{3}He. There is some disagreement with this interpretation.[14,15] Accordingly, the c^4 scaling should occur only within a short distance from P_{sl} while the c^3 scaling would be recovered at experimentally observed values of pressure. However, this seems counter to the renormalization approach where it would be expected that the exponent should be four away from the critical pressure and three some small distance from P_{sl}. At issue is whether or not the second derivative of pressure with respect to density is identically zero at the spinodal density. Recent microscopic calculations by Campbell *et al.*[17] show a different power law when very near the spinodal point. While the above discussion is limited to $T=0$ K, the c^3 scaling behavior is observed[12] for all temperatures up to the critical temperature of $T=5.2$ K.

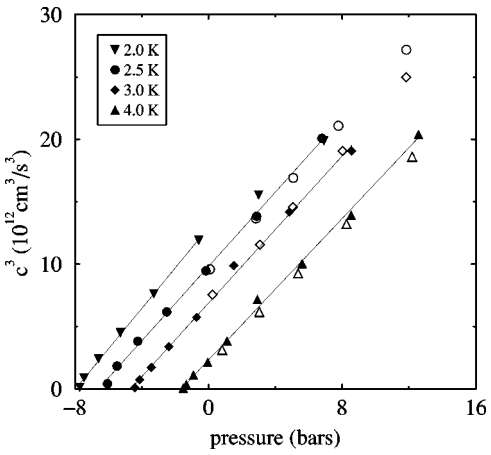

FIG. 6. The isothermal speed of sound from Eq. (7) is plotted versus pressure for varying temperature. It has been shown (Ref. 27) that c^3 should vary linearly with pressure, vanishing at the spinodal pressure. The straight lines are fits to the PIMC data (filled symbols) and are to guide the eye. The experimental data collected in Ref. 12 are indicated by the open symbols and are limited to positive pressures.

In Fig. 6 the isothermal sound velocity from PIMC simulation is plotted as a function of pressure, being determined numerically from from the PIMC pressure data

$$m_4c^2=\frac{\partial P}{\partial\rho}. \tag{7}$$

As can be seen in the figure, the PIMC data is in agreement with the relation $c^3\sim P-P_{sl}$ although there is some numerical error in taking the derivative. The experimental data exhibits a smaller slope than the simulation data but the spinodal pressures (ordinate intercept) are in agreement.

D. Excitation spectrum

The isothermal speed of sound is seen to vanish on the spinodal line. According to Maris,[12] in the quasiparticle picture of liquid helium, a transformation of the phonon branch to a free particlelike dispersion is expected to occur as the liquid spinodal line is neared. Additionally, at negative pressures, a reduction of the maxon peak may occur in the excitation spectrum. The effect of lowering the maxon peak is a spinodal pressure which has a temperature dependence similar to that in Fig. 4.

At a temperature of 1.0 K the excitation spectrum at two densities has been calculated using a maximum entropy analysis[30] on the PIMC intermediate scattering function data and is shown in Fig. 7. In this method there is a systematic error caused by the assumed entropic prior. The peaks in the calculated dynamic structure function reproduce the experimental spectrum but the calculated widths of the dynamic structure function are too large in the superfluid phase.[30] The fundamental difficulty is that the path-integral simulation must be in imaginary time to be numerically feasible for many-particle systems while the excitation spectrum is in real time. Because of the uncontrolled approximation, esti-

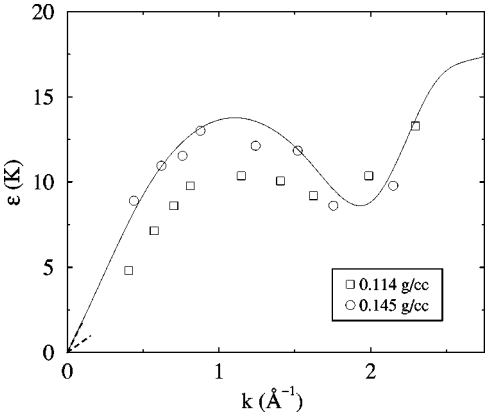

FIG. 7. The excitation spectra from PIMC simulations at a temperature of 1.0 K and densities of 0.114 g/cc and 0.145 g/cc are compared to the experimental curve (Ref. 29) (solid line). At a density of 0.114 g/cc, the system is nearly at the spinodal pressure. Tangents at $k=0$ are shown (dashed lines), where the velocity is determined by Eq. (7). The lowest value of k for the simulations is determined by the size of the computational cell.

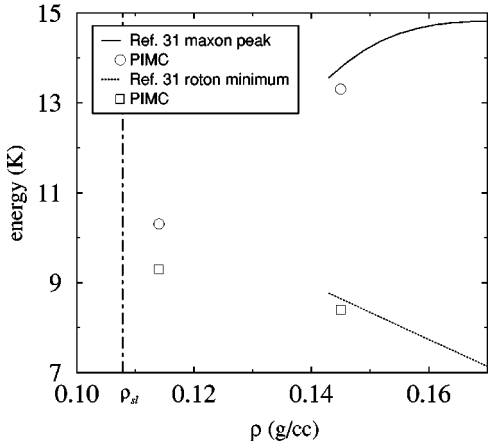

FIG. 8. The maxon peak and the roton minimum are shown as a function of density. The solid and dashed lines are fits to neutron-scattering data (Ref. 31) and the hollow symbols are the PIMC data. The trend is for the maxon peak and the roton minimum to become indistinguishable at the spinodal density (indicated by dot-dashed line).

mates for the uncertainties of the excitation energies cannot be reliably obtained. The neutron scattering data at $T<0.35$ K and density 0.145 g/cc, compiled by Donnelly,[29] is shown for comparison. The PIMC data at a density of 0.145 g/cc and pressure ~ -0.603 bar agrees with the neutron data.

The density dependence of the maxon peak and roton minimum is shown in in Fig. 8. For comparison, fits[31] to neutron data taken at nonnegative pressure are shown. At a density of 0.112 g/cc and pressure ~ -7.72 bar (very nearly the liquid spinodal density), there is a large decrease in the depth of the roton minimum with respect to the maxon peak. We predict that the roton minimum will have disappeared at the spinodal point within the accuracy of our calculation (roughly 0.5 K). The phonon part of the spectrum is at momenta less then the lowest wave vector present in the system being simulated. However, the slope of the spectrum at zero wavevector is known, Eq. (7), and is shown (dashed line) in Fig. 7 for each value of the density.

IV. CONCLUSIONS

The spinodal line, the superfluid transition and the excitation spectrum for liquid helium at negative pressures have been investigated using PIMC. The spinodal line at low temperatures shows substantial agreement with the density-functional calculations of Ref. 11 as well as at temperatures above the superfluid transition. The calculated temperature independence at low temperatures and the sudden increase in pressure as the superfluid transition is neared is consistent with the conjectures of Ref. 12. At higher temperatures there is general good agreement of the spinodal pressure with all calculations in the normal fluid phase. The superfluid transition is found to be consistent with the experimental transition values and approaches the spinodal line near 2.2 K. Finally, the excitation spectrum exhibits changes in the maxon-roton area consistent with the low-temperature behavior of the liquid spinodal line.

ACKNOWLEDGMENTS

The authors would like to acknowledge Manuel Baranco for providing their density-functional code, and Humphrey Maris for useful discussions during the course of this work. This research was supported by NASA's Microgravity Research Fundamental Physics Program, Grant No. NAG3-1926. The simulations were performed at the National Computational Science Alliance (NCSA).

[1] H. J. Maris, S. Balibar, and M. S. Pattersen, J. Low Temp. Phys. **93**, 1069 (1993).
[2] H. J. Maris, Czech. J. Phys. **46**, 2943 (1996).
[3] S. Balibar, C. Guthmann, H. Lambaŕe, P. Roche, E. Rolley, and H. J. Maris, J. Low Temp. Phys. **101**, 271 (1995).
[4] S. Balibar, F. Caupin, P. Roche, and H. J. Maris, J. Low Temp. Phys. **113**, 459 (1998).
[5] H. J. Maris, J. Low Temp. Phys. **94**, 125 (1994).
[6] S. C. Hall, J. Classen, C.-K. Su, and H. J. Maris, J. Low Temp. Phys. **101**, 793 (1995).
[7] J. Classen, C. K. Su, M. Mohazzab, and H. J. Maris, Phys. Rev. B **57**, 3000 (1998).
[8] J. Classen, C. K. Su, M. Mohazzab, and H. J. Maris, J. Low Temp. Phys. **110**, 431 (1998).
[9] H. Lambaŕe, P. Roche, S. Balibar, H. J. Maris, O. A. Andreeva, C. Guthmann, K. O. Keshishev, and E. Rolley, Eur. Phys. J. B **2**, 391 (1998).
[10] M. S. Pettersen, S. Balibar, and H. J. Maris, Phys. Rev. B **49**, 12 062 (1994).
[11] A. Guirao, M. Centelles, M. Barranco, M. Pi, A. Polls, and X. Viñas, J. Phys.: Condens. Matter **4**, 667 (1992).
[12] S. C. Hall and H. J. Maris, J. Low Temp. Phys. **107**, 263 (1997).
[13] J. Boronat and J. Casulleras, Phys. Rev. B **49**, 8920 (1994).
[14] J. Boronat, J. Casulleras, and J. Navarro, Phys. Rev. B **50**, 3427

(1994).
[15] M. A. Solís and J. Navarro, Phys. Rev. B **45**, 13 080 (1992).
[16] F. Dalfovo, A. Lastri, L. Pricaupenko, S. Stringari, and J. Treiner, Phys. Rev. B **52**, 1193 (1995).
[17] C. E. Campbell, R. Folk, and E. Krotscheck, J. Low Temp. Phys. **105**, 13 (1996).
[18] D. M. Ceperley, Rev. Mod. Phys. **67**, 279 (1995).
[19] M. C. Gordillo and D. M. Ceperley, Phys. Rev. B **58**, 6447 (1998).
[20] R. A. Aziz, A. R. Janzen, and M. R. Moldover, Phys. Rev. Lett. **74**, 1586 (1995).
[21] D. M. Ceperley and E. L. Pollock, Phys. Rev. B **39**, 2084 (1989).
[22] E. L. Pollock and K. J. Runge, Phys. Rev. B **46**, 3535 (1992).
[23] E. L. Pollock and D. M. Ceperley, Phys. Rev. B **36**, 8343 (1987).
[24] Min-Chul Cha *et al.*, Phys. Rev. B **44**, 6883 (1991).
[25] P. Grüter, D. M. Ceperley, and F. Laloë, Phys. Rev. Lett. **79**, 3549 (1997).
[26] H. J. Maris and Q. Xiong, Phys. Rev. Lett. **63**, 1078 (1989).
[27] H. J. Maris, Phys. Rev. Lett. **66**, 45 (1991).
[28] H. J. Maris (unpublished).
[29] R. J. Donnelly, J. A. Donnelly, and R. N. Hills, J. Low Temp. Phys. **44**, 471 (1981).
[30] M. Boninsegni and D. M. Ceperley, J. Low Temp. Phys. **104**, 339 (1996).
[31] J. S. Brooks and R. J. Donnelly, J. Phys. Chem. Ref. Data **6**, 51 (1977).